Super-Resolution Iris Image Restoration using Single Image for Iris Recognition

Kwang Yong Shin[1], Byung Jun Kang[2] and Kang Ryoung Park[1]
[1]Division of Electronics and Electrical Engineering, Dongguk University, Seoul, Korea
Biometrics Engineering Research Center
[e-mail: {skyandla, parkgr}@dongguk.edu]
[2]ETRI (Electronics and Telecommunications Research Institute), Daejeon, Korea,
[E-mail: kangbyj@etri.re.kr]
*Corresponding author: Kang Ryoung Park

Received January 13, 2010; revised March 2, 2010; accepted April 5, 2010; published April 29, 2010

Abstract

Iris recognition is a biometric technique which uses unique iris patterns between the pupil and sclera. The advantage of iris recognition lies in high recognition accuracy; however, for good performance, it requires the diameter of the iris to be greater than 200 pixels in an input image. So, a conventional iris system uses a camera with a costly and bulky zoom lens. To overcome this problem, we propose a new method to restore a low resolution iris image into a high resolution image using a single image. This study has three novelties compared to previous works: (i) To obtain a high resolution iris image, we only use a single iris image. This can solve the problems of conventional restoration methods with multiple images, which need considerable processing time for image capturing and registration. (ii) By using bilinear interpolation and a constrained least squares (CLS) filter based on the degradation model, we obtain a high resolution iris image with high recognition performance at fast speed. (iii) We select the optimized parameters of the CLS filter and degradation model according to the zoom factor of the image in terms of recognition accuracy. Experimental results showed that the accuracy of iris recognition was enhanced using the proposed method.

Keywords: Super-Resolution iris image, iris recognition, CLS filter

DOI: 10.3837/tiis.2010.04.003

1. Introduction

As demands for security increase, biometric identification using fingerprints, the face, the iris, and vein recognition has come into the spotlight. In practice, biometric systems have been widely used for border control, door access control, financial access, the military, and police applications. Iris recognition is one of the personal identification techniques with high confidence. Iris recognition uses unique iris patterns between the pupil and sclera for individual identification, and has high recognition accuracy due to the high degree of freedom (DOF) of iris patterns [1][2][3][4][5][6].

However, for good performance, the method requires that the diameter of the iris be greater than 200 pixels in the input image [7][8]. Therefore, the conventional iris systems often use a camera with a zoom lens [9][10][11]. Especially, the camera which is equipped with the zoom lens of longer focal length and the camera sensor of the greater number of pixels is used for iris recognition at a distance as shown in **Table 1** [8][12][13][14].

Table 1. Previous system of iris recognition at a distance

Developer	System	Stand-off Distance (meters)	Lens focal length (mm)	Sensor Resolution (pixels)
Sarnoff	Iris on the Move [8]	3	210	4 Mega
General Electric	A stand-off iris recognition system [12]	1.5	160	1,394x1,024
CASIA	Self-adaptive iris image acquisition system [13]	0.4 ~ 0.9	78	768x576
Biometrics Engineering Research Center(BERC)	Nonintrusive iris image acquisition system [14]	1.5 ~ 3	150 ~ 300	4 Mega

Compared to a conventional webcam which adopts a lens of 6 ~ 8 mm and a camera sensor of 640 x 480 pixels, the iris system of **Table 1** can become very expensive and bulky using a camera with sized zoom lens and camera sensor of large number of pixels; this prevents iris recognition systems from being widely used in many applications. To decrease cost and size, a camera without a zoom lens can be used for an iris recognition system, but this causes a reduction in recognition accuracy by capturing a low-resolution image.

Previous studies have attempted to restore a low resolution image into a high resolution image, which is called super-resolution image restoration. The super-resolution method has been applied in the surveillance, scientific, medical, and satellite imaging fields [15][16]. Most super-resolution methods are classified as reconstruction-based and learning-based [17][18]. In general, a reconstruction-based method obtains a high-resolution image based on the fusion of multiple images, whereas the learning-based method obtains it based on a model constructed by training data [17][18].

Liyakathunsia *et al.* proposed the super-resolution restoration method [19]. In order to recover the high-resolution image, the technique called blind deconvolution and zonal filters were applied to remove the blur, noise and increase the spatial resolution contained in it [19]. G. Fahmy introduced a method to restore multiple low resolution iris images into a high resolution iris image with face video of visually low resolution [20]. In case of restoring iris image, it is difficult to register multiple iris images due to the detailed patterns of iris texture,

and the contraction and dilation of the pupil area caused by variation in illumination [20].

To overcome these problems, R. Barnard *et al.* proposed the super-resolution image restoration method using a compound-eye camera equipped with multiple lenses and cameras [21]. This device can simultaneously obtain multiple low resolution iris images under the same illumination condition. However, the use of a compound-eye camera causes an iris recognition system to be costly and bulky. In previous learning-based methods, Lee *et al*. restored low-resolution face images by the support vector data description (SVDD) method based on principle component analysis (PCA) [22].

However, the PCA method using global features is inadequate for iris recognition since it uses the local feature of iris patterns. In addition, the learning-based method has the weakness that the performance of super-resolution restoration is degraded by non-trained images. Cui *et al.* used the PCA and super-resolution methods for synthesizing iris images with the objective of creating a large iris database [23]. For improved recognition accuracy and faster processing speed, Shin *et al.* proposed the restoration of a single low resolution iris image based on various image interpolations.

However, this approach has a limitation in improving the performance of iris recognition because the middle and high frequency components of a high resolution image cannot be generated only with image interpolations. Thus, they also proposed a super-resolution method based on bilinear interpolation and multiple multi-layer perceptrons (MLPs) considering three edge directions and five edge directions of the iris patterns [24][25]. The restoration method showed good performance with the trained data set, but its performance was degraded with the untrained data set. To overcome the problems of previous studies, we propose a new method to restore a single low resolution iris image into a high resolution image. To obtain a high-resolution iris image, we used a single iris image. This solves the problem of conventional restoration methods with multiple images, which need extensive processing time for image capturing and registration. We used bilinear interpolation and a constrained least squares (CLS) filter based on the degradation model to obtain a high resolution iris image with good recognition performance at fast speed. In addition, we selected the optimized parameters of the CLS filter and degradation model, which were considered by the zoom factor of the image and previously determined from the experimental results in terms of recognition accuracy.

The remainder of the paper is organized as follows. Section 2 describes the proposed method to restore a single low resolution iris image into a high resolution image. Experimental results and conclusions are described in Section 3 and Section 4, respectively.

2. Proposed System

2.1 Overview of the Method

Fig. 1 shows an overview of the proposed method. We firstly obtained a low-resolution iris image through an iris camera without a zoom lens, which can decrease the cost and size of the iris recognition system. After increasing the size of the input low-resolution iris image with bilinear interpolation, we detected the iris and pupil region using two circular edge detectors [26][27]. Next, the parameter of the degradation function was determined according to the zoom factor of the image in terms of recognition accuracy. Then, we restored the input iris image into a high resolution image based on the predetermined degradation function and the CLS filter. We selected the optimal parameters for the CLS filter and degradation function, which were previously determined from the experimental results in terms of the minimum

equal error rate (EER) of iris recognition.

Finally, Gabor wavelet-based iris recognition was performed after eliminating the eyelid and eyelashes from the restored iris image [26][28][29].

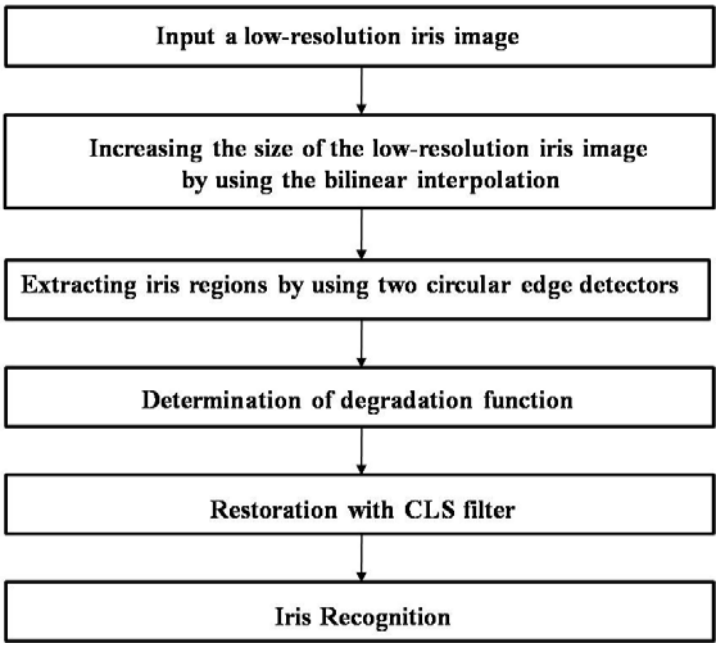

Fig. 1. Flowchart of the proposed method

2.2 Increasing the size of low-resolution image by interpolation and determination of degradation function

In general, super-resolution image reconstruction transforms multiple low resolution images into one high-resolution image [17][18]. Reconstruction using multiple images consists of three stages: image registration based on motion estimation, interpolation, and restoration. Low resolution images are registered into a reference image in the registration stage, and the low resolution images are increased to high resolution in the interpolation stage. In the restoration stage, blurring and noise are removed, and low resolution images are finally transformed into a high resolution image [17][18]. The observation model, which denotes the relationship between the low resolution images and a high-resolution image, is expressed as [17][18]:

$$\mathbf{y}_k = \mathbf{D} \cdot \mathbf{B}_k \cdot \mathbf{W}_k \cdot \mathbf{x} + \boldsymbol{\eta}_k \qquad \text{for } 1 \le k \le p \tag{1}$$

The desired high resolution image is denoted by $\mathbf{x}$ of size N in lexicographical notation as the vector $\mathbf{x} = [x_1, x_2, \ldots, x_N]^T$, for $N = L_1 N_1 \times L_2 N_2$. The parameters L_1 and L_2 represent the down-sampling factors in the horizontal and vertical directions of the observation model, respectively. The k-th low resolution image of size M is denoted by $\mathbf{y}_k$ in lexicographic notation as the vector $\mathbf{y}_k = [y_{k,1}, y_{k,2}, \ldots, y_{k,M}]^T$, for $k = 1,2,\ldots, p$ and $M = N_1 \times N_2$. The k-subscript and the p-term mean the total number of multiple low resolution images to be

restored into a single high resolution image and the sequence in multiple low resolution images, respectively. In addition, D is a $M^2 \times N$ decimation matrix, $\mathbf{W}_k$ is a $N \times N$ warp matrix by the translation and rotation of object, $\mathbf{B}_k$ denotes a $N \times N$ blur matrix that is caused by the optical blurring, motion blurring and the sensor PSF. $\boldsymbol{\eta}$ represents the additive noise vector [17][18]. Eq. (1) means that a single high resolution image can be constructed with the multiple low resolution images ($\mathbf{y}_k$ (k = 1, 2, …, p)) which were obtained from multiple cameras located in different positions or from the sequence frames of a single camera.

This paper proposes to restore a single low resolution image into a single high resolution image. In general, the translation and rotation of object are not generated in a single low resolution image but motion blurring by object motion can be only produced. So, $\mathbf{W}_k$ can be represented as an identity matrix and can be removed in Eq. (1) [17][18]. Because a single low resolution image is used, the k-subscripts of the observation model are also removed in Eq. (1). The observation model is abbreviated as:

$$\mathbf{y} = \mathbf{D} \cdot \mathbf{B} \cdot \mathbf{x} + \boldsymbol{\eta} \tag{2}$$

As shown in Eq. (2), the low resolution image is made of the blur effect ($\mathbf{B}$), the down-sampling operation (D) and the noise ($\boldsymbol{\eta}$). Therefore, the generation process of low resolution can be represented as [30]:

$$\mathbf{I}^l = (\mathbf{g} * \mathbf{I}^h) \downarrow_s + \boldsymbol{\eta} \tag{3}$$

Where $\mathbf{I}^h$ and $\mathbf{I}^l$ denote the high resolution (such as $\mathbf{x}$ in Eq. (2)) and the low resolution images (such as $\mathbf{y}$ in Eq. (2)), respectively. In addition, the $\mathbf{g}$ and "$\downarrow_s$" represent the blur effect (such as $\mathbf{B}$ in Eq. (2)) and the down-sampling operator (such as $\mathbf{D}$ in Eq. (2)), respectively. The $\mathbf{s}$ and " $*$ " mean the scaling factor and the convolution operator, respectively [30].

The down-sampling can be solved using an image interpolation method. So, the image vector $\mathbf{I}^l \uparrow_s$ which is enlarged by interpolation method is represented as:

$$\mathbf{I}^l \uparrow_s = [(\mathbf{g} * \mathbf{I}^h) \downarrow_s] \uparrow_s + \boldsymbol{\eta} \uparrow_s \tag{4}$$

Here, the "$\uparrow_s$" means the up-sampling operator using an image interpolation method. In previous research, when increasing the size of a low resolution image by various interpolation methods, recognition accuracy with the bilinear interpolation method is better than ones with other interpolation methods such as b-spline, bi-cubic, and Lanczos [25]. Thus, the bilinear interpolation method was used to solve the down-sampling in our research. Consequently, the down-sampling operator is removed by the up-sampling operator.

$$\mathbf{I}^l \uparrow_s \cong (\mathbf{g} * \mathbf{I}^h) + \hat{\boldsymbol{\eta}} \tag{5}$$

$$\hat{\mathbf{I}}^h = \mathbf{g} * \mathbf{I}^h + \hat{\boldsymbol{\eta}} \tag{6}$$

Defining $\mathbf{I}^l \uparrow_s$ as $\hat{\mathbf{I}}^h$, Eq. (5) can be represented by Eq. (6). Then, in order to decrease the processing time of restoration, we detected the iris regions by using two circular edge

detectors [26][27] with the increased image by bilinear interpolation before restoration. And the super-resolution restoration is performed only in the detected iris area. The two circular edge detectors are expressed as [26][27].

$$\max_{(x_0,y_0),r}\left[\frac{\partial}{\partial r}\left(\int_{-\frac{\pi}{4}}^{\frac{\pi}{6}}\frac{I(x,y)}{5\pi r/12}ds+\int_{\frac{5\pi}{6}}^{\frac{5\pi}{4}}\frac{I(x,y)}{5\pi r/12}ds\right)+\max_{(x'_0,y'_0),r'}\left(\frac{\partial}{\partial r'}\int_0^{2\pi}\frac{I(x',y')}{2\pi r'}ds\right)\right] \tag{7}$$

Where r and r′ represent the radii of the iris and the pupil, respectively. (x_0, y_0) and (x'_0, y'_0) represent the center positions of the iris and the pupil, respectively. Here, r, r′, (x_0, y_0) and (x'_0, y'_0) have the searching ranges, respectively, which were determined empirically. I(x, y) is the gray level of the point on the outer circular boundary of the iris, which is determined by r and (x_0, y_0). I(x', y') is the gray level of the point on the circular boundary of the pupil, which is determined by r′ and (x'_0, y'_0). The pupil and iris boundaries are determined at the position where two integro-differential values between the inner and outer edges are maximized while changing the center positions and the radius values of the pupil and iris boundaries. The range of $[0, 2\pi]$ radian is used for detecting the pupil boundary, but only the range of $[-\frac{\pi}{4}, \frac{\pi}{6}]$ radians and $[\frac{5\pi}{6}, \frac{5\pi}{4}]$ radians are for detecting the iris boundary, since it can happen that the upper or lower iris region is occluded by eyelids [26][27]. From that, by restoring only the detected iris region, we increased the restoration processing speed. Then, we explain the degradation function and how the parameters of degradation function are determined. In the spatial domain, Eq. (6) can be rewritten as [31]

$$\hat{I}^h(i,j)=h(i,j)*I^h(i,j)+\hat{\eta}(i,j) \tag{8}$$

The blur matrix $\mathbf{g}$ in Eq. (6) is represented as degradation function ($h(i,j)$), and " * " denotes a two-dimensional (2-D) convolution operator. In general, the degradation function is caused by the optical blurring, motion blurring and the sensor PSF [17][18]. Like previous researches of super-resolution restoration [19][20][21][22][23][24][25], we only consider the sensor PSF as the degradation function in this research. And it can be modeled as an uniform function as shown in Eq (9) [17] .

$$h(x,y)=\begin{cases}1/N & , if\ -\frac{z}{2}\le x\le\frac{z}{2}\ and\ -\frac{z}{2}\le y\le\frac{z}{2}\\ 0 & otherwise\end{cases} \tag{9}$$

Where z is determined by the zoom factor of the image restoration, and N is the magnitude of the uniform function and is defined as z × z. (For example, if we try to double the size of the original image, z is 2 and N is 4.) In our experiments, we considered zoom-in factors of 2 to 5. For a zoom-in factor of 2 or 4, phase distortion is generated when the degradation function in the spatial domain is transformed into the frequency domain because a digital image is discrete [32]. Therefore, we substituted the degradation functions of 2 × 2 and 4 × 4 with 3 × 3 and 5 × 5, respectively, to solve the phase distortion problem, as shown in **Fig. 2**, **Table 3**, **Table 4** and **Table 6**.

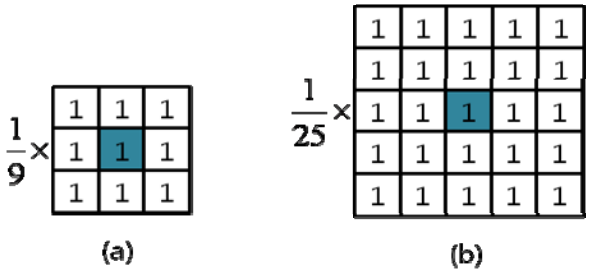

Fig. 2. Uniform degradation function: (a) 3x3 uniform function, and (b) 5x5 uniform function

From Eq. (8), the de-convolution operation was performed to obtain the high resolution image ($I^h(i,j)$). Thus, the convolution operation was converted into a multiplication operation by transforming the image in the spatial domain into an image in frequency domain [31]. Equation (8) is expressed as

$$\hat{I}^h(u,v) = H(u,v) \cdot I^h(u,v) + \hat{N}(u,v) \tag{10}$$

Here, $I^h(u,v)$, $\hat{I}^h(u,v)$ and $\hat{N}(u,v)$ are the original high resolution image, the low resolution image with up-sampling, and the noise in frequency domain, respectively. $H(u,v)$ is the modulation transfer function (MTF) and the degradation function in the frequency domain. $H(u,v)$ is represented as a sinc function because a rectangular function from Eq. (9) is transformed into a sinc function in the frequency domain as shown in **Fig. 3** [33].

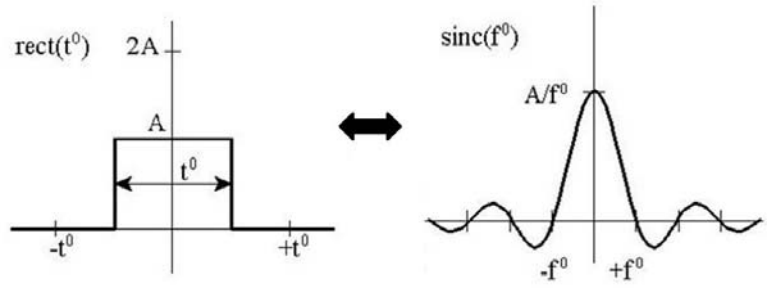

Fig. 3. Rectangular function in spatial domain and sinc function in frequency domain

2.3 Restoration with CLS filter

To obtain a high resolution image without the blurring caused by low resolution, we used a constrained least square (CLS) filter. In general, an inverse filter can be derived as described by Eq. (11) without the noise term ($\hat{N}(u,v)$) of Eq. (10) [31].

$$I^h(u,v) = \left[\frac{H^*(u,v)}{|H(u,v)|^2} \right] \hat{I}^h(u,v) \tag{11}$$

However, the additive noise ($\hat{N}(u,v)$) should be considered since it is actually generated while capturing an iris image. Because the blurring function, ($H(u,v)$ of Eq. (10)), is a low frequency

component and the additive noise is a high frequency component, a high-pass filter is required to reduce the effect of the blurring function. A low-pass filter is commonly required for the reduction of additive noise [31].

Reducing the blurring function conflicts with the reduction of additive noise; thus, an optimization strategy is required to obtain a high resolution image [34]. The CLS filtering method provides the optimization strategy, as shown in Eq. (12).

$$I^h(u,v) = \left[\frac{H^*(u,v)}{|H(u,v)|^2 + \alpha|L(u,v)|^2}\right]\hat{I}^h(u,v) \tag{12}$$

Where α denotes the regularization parameter that controls the tradeoff between the fidelity of the clear image with the high frequency component and the reduction in additive noise. $L(u,v)$ denotes the Fourier transform of the high-pass filter. We used a Laplacian filter for $L(u,v)$. The eq. (12) of the proposed method is completely different from that in the previous work [34] in terms of the role of the equation, the PSF and the method of acquiring the optimal parameters.

In the previous work [34], the CLS filter was used for restoring the optically blurred iris image. So, the Gaussian function was used as the point spread function (PSF) of the CLS filter in [34]. And the optimal sigma parameter of the Gaussian function and the optimal regularization parameter of the CLS filter (α of eq. (12)) were determined based on the measured focus score of the iris image by using a 5x5 convolution mask irrespective of the zoom-out factor of input image in [34].

However, the CLS filter of eq. (12) in our research is used to restore the blurring caused by camera sensor. So, the uniform function like **Fig. 2** is used as the PSF ($H(u, v)$) of the CLS filter of eq. (12) since it has been mostly used as the PSF of the blurring by camera sensor in the previous researches of super-resolution restoration [19][20][21][22][23][24][25]. The optimal size of the PSF and the optimal parameter (α) of the CLS filter of eq. (12) were empirically determined (as shown in **Table 3**) according to the zoom-out factors of the low resolution image in terms of iris recognition accuracy.

2.4 Iris recognition

After changing a low resolution iris image into a high resolution image, the eyelid candidate points were extracted with an eyelid detecting mask as shown in **Fig. 4**. The upper and lower eyelid curves were fitted using a parabolic Hough transform and the detected eyelid candidate points [28]. Eyelashes, which have the features of vertical direction and a lower gray level than the neighboring pixels, were detected using eyelash detecting masks based on these features [29].

Next, the preprocessed iris region shown in **Fig. 4**(b) was transformed into a rectangular image with 256 sectors and 8 tracks, as shown in **Fig. 4**(c) [1][2][3][35]. And then, a Gabor wavelet filter was used to extract the binary iris codes of 2,048 bits. In general, the size and the wavelength parameters of the Gabor filter affect the accuracy of iris recognition; the Gabor filter having high frequency and small kernel size leads to good recognition performance at the iris image with fine texture information while that having low frequency and large kernel size is used to enhance recognition performance at iris images with blurred or low texture information [35].

Experimental results with CASIA database showed that when the kernel size and frequency of the Gabor filter were 25 and 1/20 respectively, the recognition accuracy was highest [35]. We also extracted the mask code of 2,048 bits; this represented whether or not the extracted

binary iris codes were from the iris region un-occluded by the eyelid, eyelashes, and pupil (only the iris codes from the un-occluded iris region were used for calculating the Hamming Distance (HD)).

From the experimental results, we determined the threshold of the HD (0.34) from which the minimum EER of iris recognition was obtained in order to discriminate between genuine and imposter data. If the calculated HD was less than the threshold, the input iris image was accepted as a genuine image. If the HD was greater than the threshold, it was rejected as an imposter image.

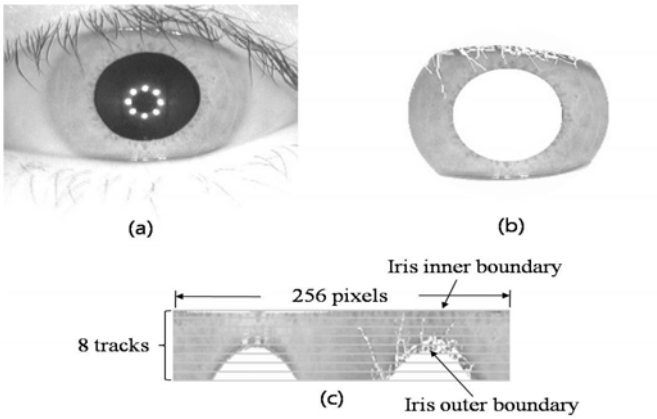

Fig. 4. An example of Gabor wavelet-based iris recognition: (a) iris image, (b) preprocessed image, and (c) rectangular image in polar coordinates

3. Experimental Results

To test our proposed method, we used the public iris image database of CASIA Interval Version 3 [36]. The iris image databases of CASIA Interval are composed of 2,655 images acquired from 396 classes of 249 volunteers. The image size is 320×280 pixels with 8-bit gray levels. To test the performance of the proposed method, we produced low resolution images according to a zoom-out factor of 1/2 to 1/5. For a zoom-out factor of 1/2, the horizontal and vertical sizes of the original iris image were reduced by half. Therefore, we can obtain that the 160×140 low resolution images had 25% as many pixels as the original images. In case of 11%, 6% and 4% of the low resolution images, 106×93, 80×70 and 64×56 low resolution images had 11%, 6% and 4% as many pixels as the original images of the CASIA Interval database using the decimation and bilinear interpolation method, respectively. **Fig. 5** shows low resolution images at zoom-out factors from 1/2 to 1/5.

Table 2. EER with low resolution iris images using decimation and bilinear interpolation method at zoom-out factors from 1/2 to 1/5

Resolution of Iris image at zoom-out factors	EER(%)
320×280 image (original)	0.886
160×140 image (zoom-out factor of 1/2)	4.064
106×92 image (zoom-out factor of 1/3)	14.253
80×70 image (zoom-out factor of 1/4)	25.156
64×56 image (zoom-out factor of 1/5)	32.916

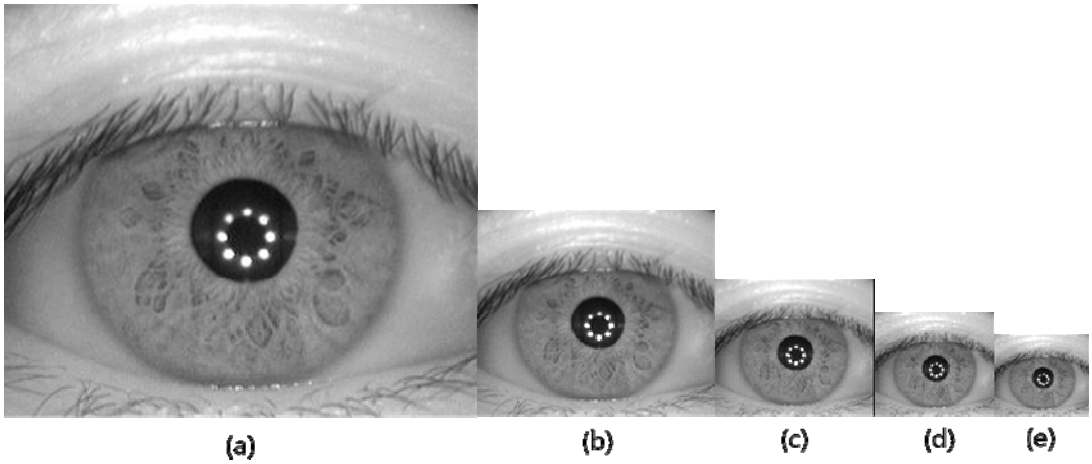

Fig. 5. Iris image at zoom-out factors from 1/2 to 1/5: (a) 320×280 image (original); (b) 160×140 image (zoom-out factor of 1/2); (c) 106×93 image (zoom-out factor of 1/3); (d) 80×70 image (zoom-out factor of 1/4); and (e) 64×56 image (zoom-out factor of 1/5).

According to zoom-out factors, we measured the EER at the low resolution images which were produced by using the decimation and bilinear interpolation method as shown in **Table 2** [25]. In a matching process for recognition, the low resolution image and original image were used as an input image and an enrolled image, respectively. In other words, the HDs between the low resolution images and the original images were calculated for user identification. The EER was obtained through 2,255 genuine tests and 845,333 imposter tests. As shown **Table 2**, the lower resolution the iris image has, the more the accuracy of iris recognition is reduced. That is why the decrement of the spatial resolution causes the loss of the iris pattern information.

After enlarging low resolution images by the bilinear interpolation method, we selected an image of 256×256 pixels from the center of the iris region as shown in **Fig. 6** in order to reduce the computational time of the Fast Fourier Transform (FFT). In the frequency domain, a single low resolution image was restored into a single high resolution image by using the CLS filtering method as shown in Eq. (12). In the restoration process, we determined the optimal size of the degradation function and the optimal value of the regularization parameter empirically, as shown in **Table 3**. We also substituted the degradation functions of 2 × 2 pixels and 4 × 4 pixels with 3 × 3 pixels and 5 × 5 pixels, respectively, to avoid phase distortion, as explained in Section 2.2.

In general, the lower resolution the iris image has, the more the loss of the high frequency component is increased. In order to compensate for the loss, the regularization parameter of CLS filter is decreased according to the zoom-out factors of 1/2 to 1/5 as shown in **Table 3**. As shown in Eq. (12), the small regularization parameter decreases the passing amount of high frequency components.

However, the high pass filter exists in the denominator of Eq. (12) and the reduction of regularization parameter increases the whole amount of high frequency components, consequently.

However, the regularization parameter value of CLS filter was suddenly increased in case that the zoom-out factor was 1/5. When the 4% low resolution image was restored with a smaller regularization parameter, there happened much amount of angularities in the pupil boundary as shown in **Fig. 7(b)**, which increased the segmentation error of pupil region and

the consequent error of iris recognition. As shown in **Fig. 7(c)**, the amount of angularity was reduced when the larger regularization parameter was used. So, the recognition accuracy was highest at which the regularization parameter value was 2.47 as shown in **Table 7**. **Fig. 8** shows iris images restored using the proposed method.

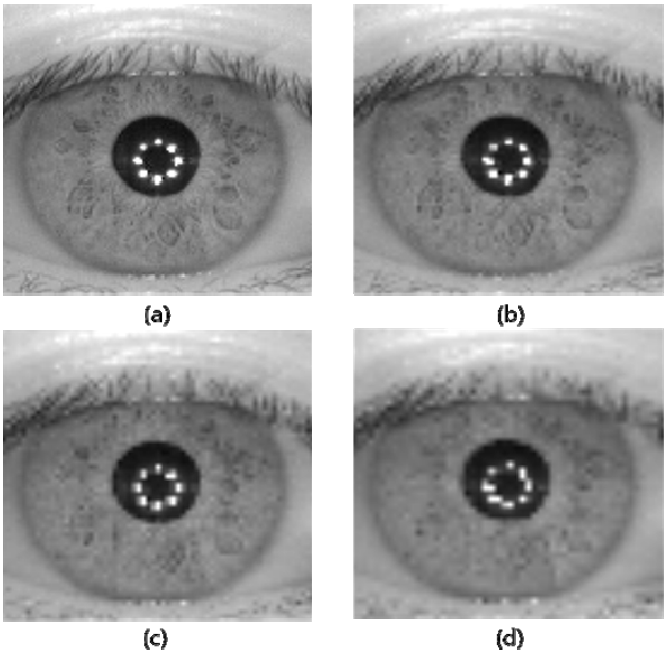

Fig. 6. Enlarged images by bilinear interpolation (256 x 256 pixels): (a) enlarged image from 25% low resolution (**Fig. 5 (b)**); (b) enlarged image from 11% low resolution (**Fig. 5 (c)**); (c) enlarged image from 6% low resolution (**Fig. 5 (d)**); and (d) enlarged image from 4% low resolution (**Fig. 5 (e)**)

Table 3. Optimal degradation function and regularization parameter of CLS filter along zoom-out factor

Zoom factor of camera	The degradation function ($H(u,v)$ in Eq. (12))	The regularization parameter of CLS filter (α in Eq. (12))
1/2 (25% low resolution)	3×3 pixels uniform function	2.15
1/3 (11% low resolution)	3×3 pixels uniform function	2.05
1/4 (6% low resolution)	5×5 pixels uniform function	0.4
1/5 (4% low resolution)	5×5 pixels uniform function	2.47

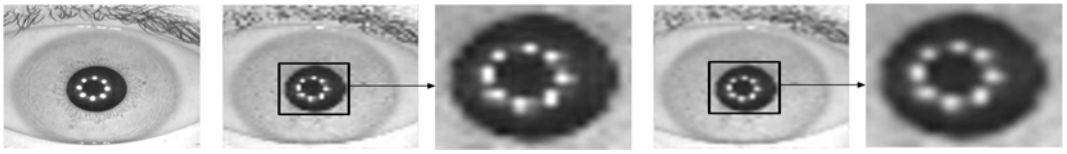

Fig. 7. Examples of restored iris images of 4% low resolution (256×256 pixels): (a) original iris image; (b) the restoration result when the regularization parameter value (α) of CLS filter is 0.3; (c) the restoration result when the regularization parameter value (α) of CLS filter is 2.47

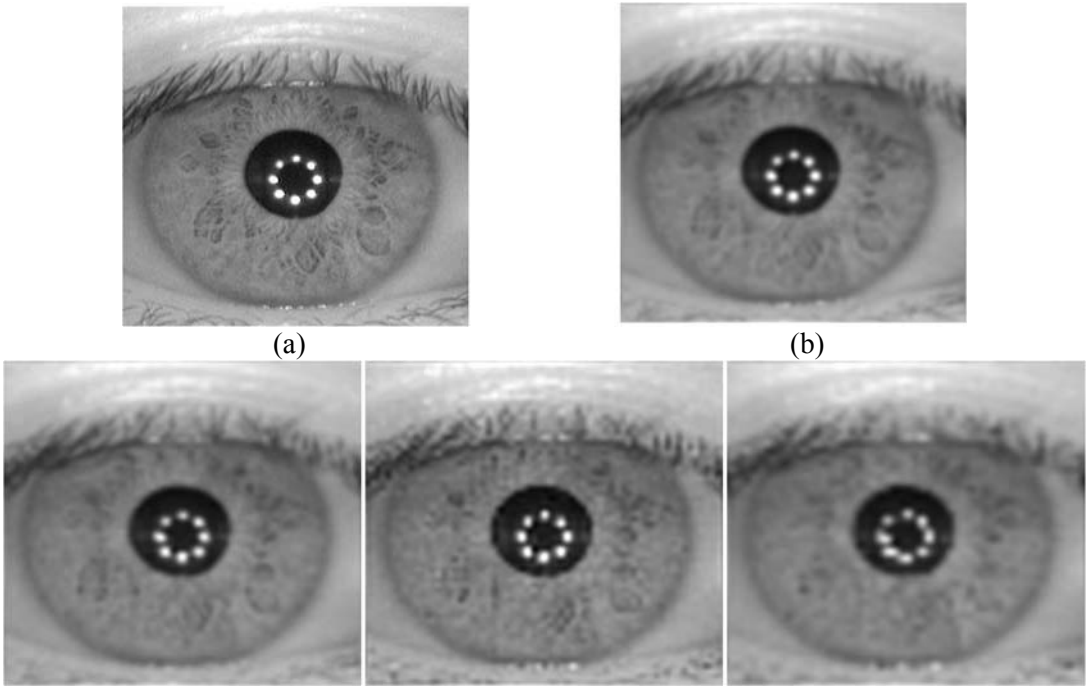

Fig. 8. Examples of restored iris images (256×256 pixels): (a) original iris image; (b) restored iris image of 25% low resolution (**Fig. 6(b)**); (c) restored iris image of 11% low resolution (**Fig. 6(c)**); (d) restored iris image of 6% low resolution (**Fig. 6(d)**); and (e) restored iris image of 4% low resolution (**Fig. 6(e)**)

In the first experiment, we tested the performance of the proposed method with the restored images using 25% low resolution. In case of 25% low resolution, 3x3 pixels uniform function and 2.15 of the regularization parameter (α) value of CLS filter were used for restoring 25% low resolution image to high resolution image.

We included the two comparisons with the existing methods. In the first test, we compared the performance of the proposed method with those of the various interpolation methods such as b-spline, bi-cubic, lanczos2 and lanczos3 interpolations at each low resolution image. The lanczos2 and lanczos3 interpolations use 4x4 and 6x6 masks of sinc functions, respectively. As shown in **Table 4~7** and **Fig. 9~12** the accuracy of iris recognition by the proposed method was better than the conventional interpolations such as b-spline, bi-cubic, lanczos2 and lanczos3 interpolations.

In the next test, we compared the performance of the proposed method with that of previous work [19]. In order to recover the high-resolution image, the technique called blind deconvolution and zonal filters were applied to remove the blur, noise and increase the spatial resolution contained in it [19]. As shown in **Table 4~7** and **Fig. 9~12**, the accuracy of iris recognition by the proposed method was better than the method of [19].

Table 4 shows the EER with the restored images using 25% low resolution images. The EER of the 25% low resolution image increased by as much as 3.178% (4.064% − 0.886%) compared to the original images due to the loss of iris pattern information. As shown in **Table 4**, the recognition accuracy of each interpolation was better than that of low resolution image. Also, the recognition accuracy of b-spline interpolation was better than other interpolations as shown in **Table 4** and **Fig. 9(a)**. **Fig. 9(a)** and **Fig. 9(b)** show the receiver operational characteristic (ROC) curves with the genuine acceptance rate (GAR) (= 100 – FRR (%)) at a

variable false rejection rate (FRR). FRR is the error rate of rejecting a genuine user as an imposter user. The false acceptance rate (FAR) is the error rate of accepting an imposter user as a genuine user. The recognition accuracy of restored images using blind restoration method [19] is higher than that of b-spline interpolation as shown in **Table 4** and **Fig. 9(b)** Our proposed method, however, showed better accuracy than blind restoration method [19] as shown in **Table 4** and **Fig. 9(b)**.

Table 4. EER at the 25% low resolution images

Resolution of Iris image	EER(%)
Original image (320×280 pixels)	0.886
Low resolution image (160×140 pixels)	4.064
B-spline interpolation	1.329
Bi-cubic interpolation	1.485
Lanczos2 interpolation	1.383
Lanczos3 interpolation	1.373
Restored image by blind restoration [19]	1.037
Restored image by the proposed method (based on 3×3 pixels uniform function, 2.15 of α value)	0.936

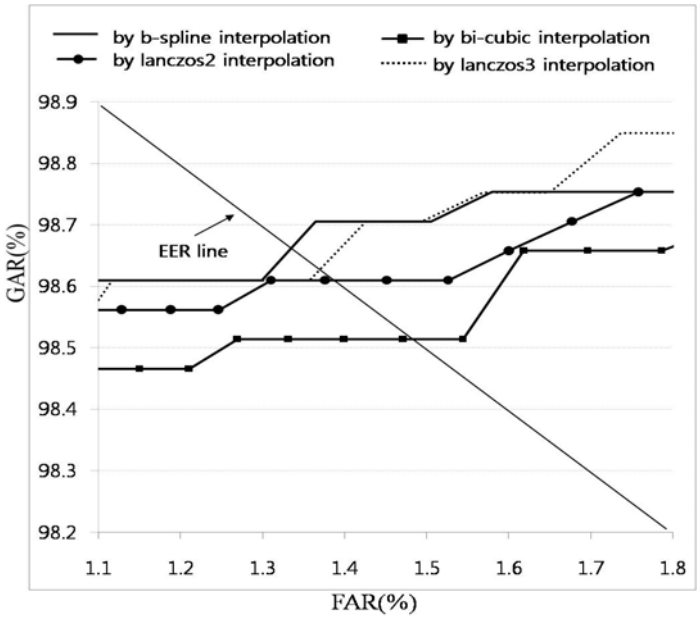

(a)

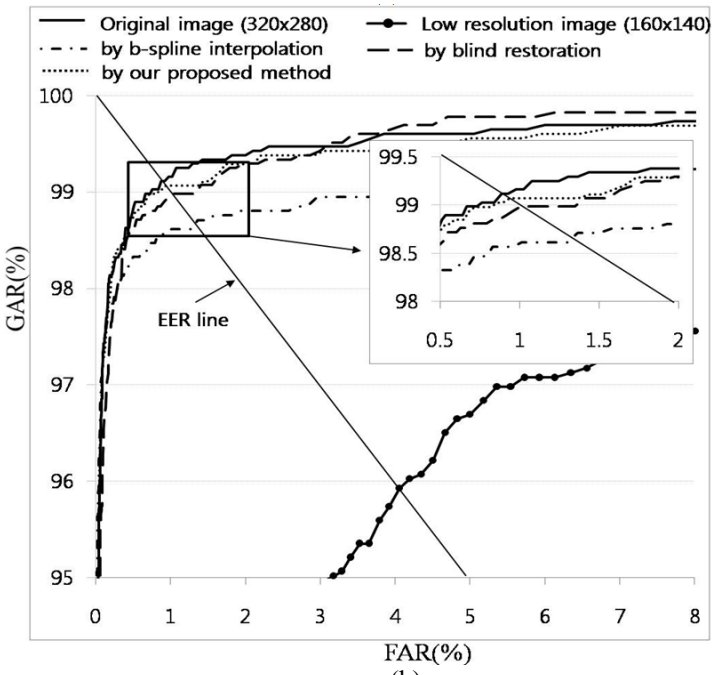

(b)

Fig. 9. ROC curves at 25% low resolution image: (a) ROC curves by each interpolation, (b) ROC curves of the proposed method compared to other methods

In the second experiment, we tested the performance of the proposed method with restored images for 11% low resolution images. In case of 11% low resolution, 3x3 pixels uniform function and 2.05 of the regularization parameter (α) value of CLS filter were used. **Table 5** shows the EER with restored images for 11% low resolution images. The EER of the 11% low resolution image increased as much as 13.367% (14.253% − 0.886%) in comparison with the EER of the original images. The accuracy of iris recognition by the proposed method was better than those of low resolution image and other methods as shown in **Table 5** and **Fig. 10**.

Table 5. EER at the 11% low resolution images

Resolution of Iris image	EER(%)
Original image (320×280 pixels)	0.886
Low resolution image (106×93 pixels)	14.253
B-spline interpolation	1.350
Bi-cubic interpolation	1.437
Lanczos2 interpolation	1.881
Lanczos3 interpolation	1.884
Restored image by blind restoration [19]	1.053
Restored image by the proposed method (based on 3×3 pixels uniform function, 2.05 of α value)	0.951

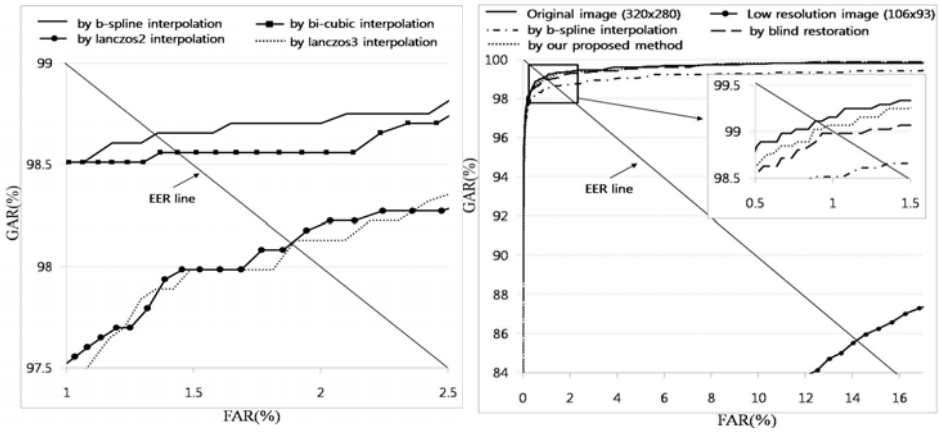

(a) (b)

Fig. 10. ROC curves at 11% low resolution image: (a) ROC curves by each interpolation, (b) ROC curves of the proposed method compared to other methods

In the third experiment, we tested the performance of the proposed method for 6% low resolution images. In case of 6% low resolution, 5x5 pixels uniform function and 0.4 of the regularization parameter (α) value of CLS filter were used.

In the fourth experiment, the performance of the proposed method for 4% low resolution images was measured using 5x5 pixels uniform function and 2.47 of the regularization parameter (α) value of CLS filter. **Table 6** and **Table 7** show EERs with the restored images for the 6% low resolution images and the 4% low resolution images, respectively.The EER of the 6% low resolution images was 25.156% and the EER of the 4% low resolution images was 32.916%. Lower spatial resolution resulted in lower recognition accuracy because the amount of lost information increased. We compared the performance of the proposed method with those of the previous methods. The accuracy of iris recognition by the proposed method was better than those of low resolution image and other methods as shown in **Table 6**, **Table 7** and **Fig. 11**, **Fig. 12**.

Table 6. EER at the 6% low resolution images

Resolution of Iris image	EER(%)
Original image (320×280 pixels)	0.886
Low resolution image (80×70 pixels)	25.156
B-spline interpolation	1.744
Bi-cubic interpolation	1.840
Lanczos2 interpolation	2.205
Lanczos3 interpolation	2.276
Restored image by blind restoration [19]	1.427
Restored image by the proposed method (based on 5×5 pixels uniform function, 0.4 of α value)	1.322

Table 7. EER at the 4% low resolution images

Resolution of Iris image	EER(%)
Original image (320×280 pixels)	0.886
Low resolution image (64×56 pixels)	32.916
B-spline interpolation	1.898
Bi-cubic interpolation	2.705
Lanczos2 interpolation	2.818
Lanczos3 interpolation	2.793
Restored image by blind restoration [19]	1.747
Restored image by the proposed method (based on 5×5 pixels uniform function, 2.47 of α value)	1.641

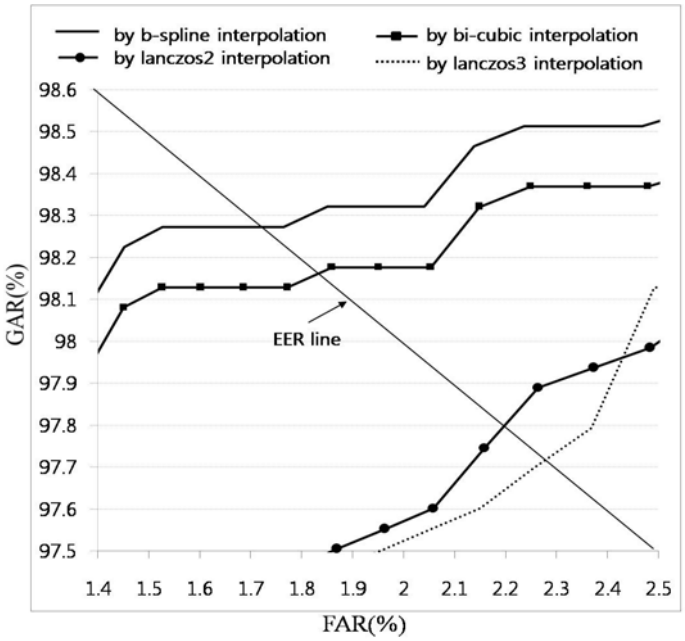

(a)

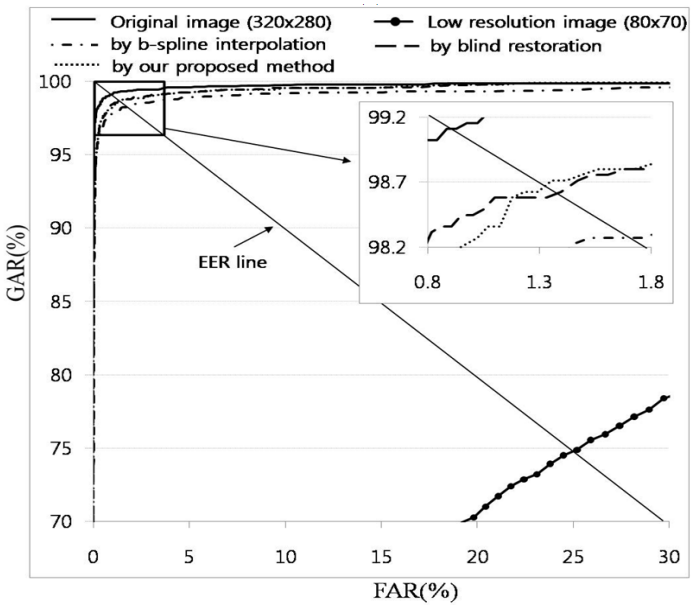

(b)

Fig. 11. ROC curves at 6% low resolution image: (a) ROC curves by each interpolation, (b) ROC curves of the proposed method compared to other methods

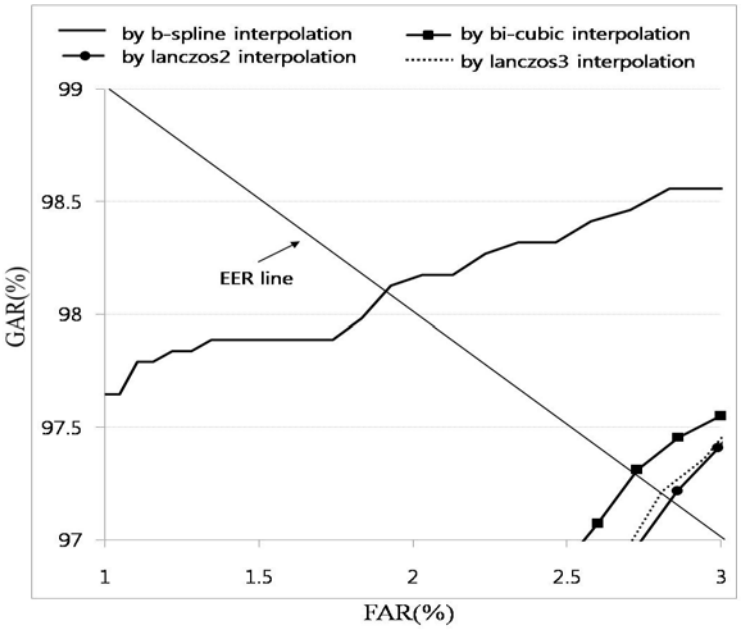

(a)

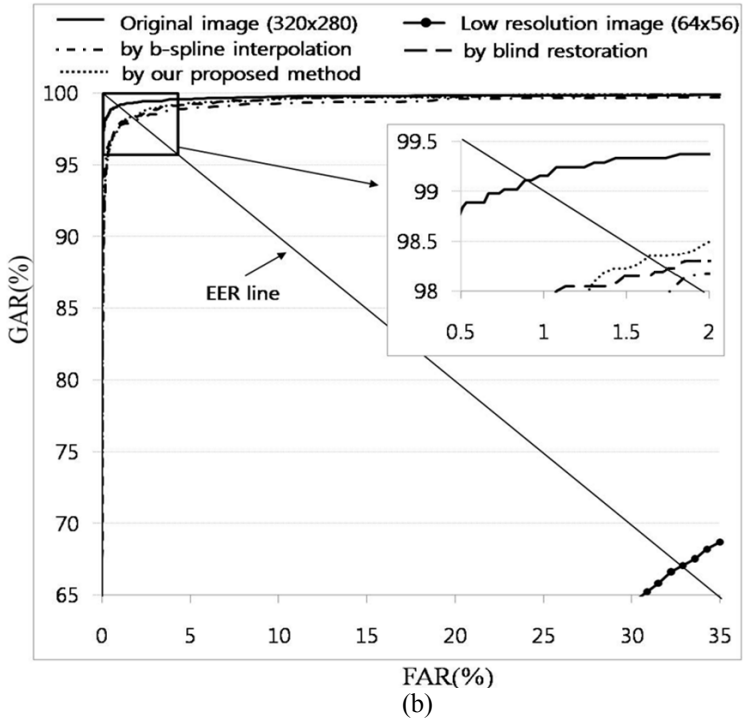

Fig. 12. ROC curves at 4% low resolution image: (a) ROC curves by each interpolation, (b) ROC curves of the proposed method compared to other methods

In the final experiment, we measured the processing time of our proposed method on a desktop computer with a 2.33 GHz Intel Core™ 2 Quad processor. As shown in **Table 8**, the processing time for bilinear interpolation was 4.2 ms and the processing time for the proposed iris image restoration was 24.6 ms. Thus, it is possible for the proposed restoration method to be applied in a real-time system. The total processing time including iris recognition was 292.4 ms.

Table 8. Processing time

	Bilinear interpolation	Restoration with CLS filter	Iris recognition	Total
Processing time (ms)	4.2	24.6	263.6	292.4

4. Conclusions

We proposed a new method to restore a single low resolution iris image into a high resolution iris image. The processing time of proposed method is much smaller than conventional restoration method using multiple low resolution images, since the proposed method only uses a single image.

The proposed method obtains a high resolution iris image with high recognition performance using the bilinear interpolation and constrained least squares (CLS) filter based on the degradation model. By restoring only the detected iris region, we increased the restoration processing speed. Experimental results using the "Interval" images from the CASIA database (version 3) showed that recognition accuracy using the proposed method was greatly enhanced compared to low resolution images and other methods. In future work, we plan to study the restoration of a low resolution image with motion and optical blurring.

Acknowledgement

This work was supported by the Korea Science and Engineering Foundation (KOSEF) through the Biometrics Engineering Research Center (BERC) at Yonsei University [R112002105070020(2009)]. “Portions of the research in this paper use the CASIA-IrisV3 collected by the Chinese Academy of Sciences’Institute of Automation (CASIA)” and a reference to "CASIA-Iris V3, http://www.cbsr.ia.ac.cn/IrisDatabase.htm”.

References

[1] J. G. Daugman, "High Confidence Visual Recognition of Personals by a Test of Statistical Independence," *IEEE Trans. on Pattern Analysis and Machine Intelligence*, vol.15, no.11, pp. 1148-1160, 1993.
[2] J. G. Daugman, "Demodulation by Complex-valued Wavelets for Stochastic Pattern Recognition,” *International Journal of Wavelets*, vol.1, no.1, pp.1-17, 2003.
[3] J. G. Daugman, "How Iris Recognition Works," *IEEE Trans. on Circuits and Systems for Video Technology*, vol.14, no.1, pp.21-30, 2004.
[4] International Biometrics Group, Independent Testing of Iris Recognition Technology Final Report, 2005. http://www.biometricscatalog.org/document_area/default.aspx (accessed on January 4, 2010).
[5] R. P. Wildes, “Automated Iris Recognition: An Emerging Biometric Technology,” *Proceedings of the IEEE*, vol.85, no.9, pp.1348-1363, 1997.
[6] R. P. Wildes, "Iris Recognition," *Biometric Systems*m, pp. 63-95, 2005.
[7] Information Technology, “Biometric Data Interchange Formats - Iris Image Data,” *ISO/IEC 19794-6*, 2005.
[8] J. R. Matey, O. Naroditsky, K. Hanna, R. Kolczynski, D. LoIacono, S. Mangru, M. Tinker, T. Zappia, and W.Y. Zhao, “Iris on the Move: Acquisition of Images for Iris Recognition in Less Constrained Environments,” *Proceedings of the IEEE*, vol.94, pp.1936-1946, 2006.
[9] IrisAccess 4000. http://www.lgiris.com/ps/products/index.htm (accessed on January 4, 2010).
[10] IrisPass-M. http://www.oki.com/jp/FSC/iris/en/index.html (accessed on January 4, 2010).
[11] BM-ET 200. http://www.panasonic.com/business/security/biometrics.asp (accessed on January 4, 2010).
[12] Frederick W. Wheeler, A. G. Amitha Perera, Gil Abramovich, Bing Yu, and Peter H. Tu, “Stand-off Iris Recognition System,” in *Proc. 2nd Int IEEE Conf of. On Biometrics:Theory, Applications and Systems*, pp.1-7, 2008.
[13] Wenbo Dong, Zhenan Sun, Tieniu Tan, and Xianchao Qiu, “Self-adaptive Iris Image Acquisition System,” in *Proc. of the SPIE Biometric Technology for Human Identification*, vol.6944, pp.6-14, 2008.
[14] Soweon Yoon, Ho Gi Jung, Kang Ryoung Park and Jaihie Kim, “Non-intrusive Iris Image Acquisition System Based on a Pan-Tilt-Zoom Camera and Light Stripe Projection,” *Optical Engineering*, vol.48, no.3, pp.137202-1 - 137202-15, 2009.
[15] F. Lin, C. Fookes, V. Chandran, and S. Sridharan, “Investigation into Optical Flow Super-Resolution for Surveillance Applications,” in *Proc. of APRS Workshop on Digital Image Computing*, pp.73–78, 2005.
[16] H. Greenspan, G. Oz, N. Kiryati and S. Peled, “MRI Inter-Slice Reconstruction Using Super Resolution,” *Magnetic Resonance Imaging*, vol.20, pp.437-446, 2002.
[17] S. C. Park, M. K. Park, and M. G. Kang, “Super-resolution Image Reconstruction: a Technical Overview,” *IEEE Signal Processing Magazine*, vol.20, no.3, pp.21-36, May 2003.
[18] D. Capel and A. Zisserman, “Computer Vision Applied to Super-resolution,” *IEEE Signal Processing Magazine 20*, pp.75 -86, 2003.
[19] Liyakathunisa, and V.K. Anantha Shayana “Super Resolution Blind Restoration of Noisy, Blurred and Aliased Low Resolution Images under Compression,” in *Proc. of Int Conf of. on Information*

Systems, pp.61-66, 2007.
[20] G. Fahmy, "Super-resolution Construction of IRIS Images from a Visual Low Resolution Face Video," In *Proc. of International Symposium on Signal Processing and its Applications*, pp.1-4, 2007.
[21] R. Barnard et al., "High-Resolution Iris Image Reconstruction from Low-Resolution Imagery", in *Proc. of the SPIE, Advanced Signal Processing Algorithms, Architectures, and Implementations XVI*, vol. 6313, pp. D1-D13, 2006.
[22] S. W. Lee, J. Y. Park and S.W. Lee, "Low Resolution Face Recognition Based on Support Vector Data Description," *Pattern Recognition*, vol.39, no.9, pp. 1809-1812, 2006.
[23] Jiali. Cui, Yunhong Wang, Junzhou. Huang, Tieniu Tan, and Zhenan Sun, "An Iris Image Synthesis Method based on PCA and Super-resolution," in *Proc. of 17th Int Conf. on Pattern Recognition*, vo.4, pp.471–474, 2004.
[24] K. Y. Shin, B. J. Kang, and K. R. Park, "Super-Resolution Method Based on Multiple Multi-Layer Perceptrons for Iris Recognition," in *Proc. of the* 4th *Int Conf. on Ubiquitous Information Technologies & Applications*, 2009.
[25] K. Y. Shin, B. J. Kang, and K. R. Park, "A Study on the Restoration of a Low-Resoltuion Iris Image into a High-Resolution One Based on Multiple Multi-Layered Perceptrons," *Korea Multimedia Society*, Mar 2010, accepted for publication.
[26] D. H. Cho, K. R. Park, D. W. Rhee, Y. G. Kim, and J. H. Yang, "Pupil and Iris Localization for Iris Recognition in Mobile Phones," in *Proc. of SNPD 2006*, 2006.
[27] D. S. Jeong, J. W. Hwang, B. J. Kang, K. R. Park, C. S. Won, D. K. Park, and J. Kim, "A New Iris Segmentation Method for Non-ideal Iris Images," *Image and Vision Computing*, 2010, accepted for publication.
[28] Y. K. Jang, B. J. Kang, and K. R. Park, "A Study on Eyelid Localization Considering Image Focus for Iris Recognition," *Pattern Recognition Letters*, vol.29, no.11, pp.1698-1704, 2008.
[29] B. J. Kang, and K. R. Park, "A Robust Eyelash Detection Based on Iris Focus Assessment," *Pattern Recognition Letters*, vol.28, no.13, pp.1630-1639, 2007.
[30] S. Dai, M. Han, Y. Wu, and Y. Gong, "Bilateral Back-Projection for Single Image Super Resolution" in *Proc. of Int. Conf. on Multimedia and Expo*, pp.1039-1042, 2007.
[31] R. C. Gonzalez, and R. E. Woods, Digital Image Processing, 2/E, *Prentice Hall*, 2002.
[32] M. Manry, and J. Aggarwal, "The Measurement of Phase Distortion Due to Filtering in Digital Pictures," *IEEE Trans. on Acoust*., vol.ASSP-25, pp.534-541, 1977.
[33] R. Lokhande, K. V. Arya, and P. Gupta, "Identification of Parameters and Restoration of Motion Blurred Images," in *Proc. of the 2006 ACM Symposium on Applied Computing*, pp.301-305, 2006.
[34] B. J. Kang, and K. R. Park, "Real-time Image Restoration for Iris Recognition Systems," *IEEE Trans. on Systems*, vol.37, no.6, pp.1555-1566, 2007.
[35] Hyun-Ae Park, and Kang Ryoung Park, "Iris Recognition Based on Score Level Fusion by Using SVM," *Pattern Recognition Letters*, vol.28, no.15, pp.2019-2028, 2007.
[36] CASIA ver. 3. http://www.cbsr.ia.ac.cn/IrisDatabase.htm (accessed on January 4, 2010)

Kwang Yong Shin received a B.S. degree in digital media from Dongguk University, Seoul, South Korea, in 2009. He is currently pursuing a M.S. degree in Electronics Engineering at Dongguk University. He is also a research member of Biometrics Engineering Research Center. His research interests include biometrics and image processing.

Byung Jun Kang received B.S. and M.S. degrees in Software and Computer Science from Sangmyung University, Seoul, South Korea, in 2004 and 2006 respectively. In 2009, he also earned a Ph.D degree in Computer Science from the Department of Computer Science of Sangmyung University, Seoul, South Korea. He is currently a Researcher at the Electronics and Telecommunications Research Institute. His research interests include biometrics and image processing

Kang Ryoung Park received his BS and MS degrees in electronic engineering from Yonsei University, Seoul, Korea, in 1994 and 1996, respectively. He also received his PhD degree in computer vision from the Department of Electrical and Computer Engineering in Yonsei University in 2000. He was an assistant professor in the Division of Digital Media Technology at Sangmyung University from March 2003 to February 2008. He has been an assistant and associate professor in the Department of Electronics Engineering at Dongguk University since March 2008. He is also a research member of BERC. His research interests include computer vision, image processing, and biometrics.